International Journal of Nanomedicine

Dovepress
Taylor & Francis Group

Open Access Full Text Article

ORIGINAL RESEARCH

Enhancing the Antidepressant Efficacy of Quercetin via Brain-Targeted Lipid Nanocarriers: Fabrication, Characterization, and Evaluation

Tao Chen[1], Mingtang Zeng[2], Linjin Xiong[3], Wen Li[4], Zhichan Cheng[5], Chenglong Wang[1]

[1]Department of Pharmacy, Yibin Hospital Affiliated to Children's Hospital of Chongqing Medical University, Yibin, Sichuan, People's Republic of China; [2]Department of Pharmacy, West China Hospital, Sichuan University, Chengdu, Sichuan, People's Republic of China; [3]Department of Pharmacy, Chengdu Hi-Tech Zone Hospital for Women and Children (Chengdu Hi-Tech Zone Hospital for Maternal and Child Healthcare), Chengdu, Sichuan, People's Republic of China; [4]School of Pharmacy, Central Nervous System Drug Key Laboratory of Sichuan Province, Southwest Medical University, Luzhou, Sichuan, People's Republic of China; [5]Department of Pharmacy, Chongqing Emergency Medical Center, Chongqing University Central Hospital, Chongqing, People's Republic of China

Correspondence: Chenglong Wang, Department of Pharmacy, Yibin Hospital Affiliated to Children's Hospital of Chongqing Medical University, No. 108, Shangmao Road, Xuzhou District, Yibin, Sichuan, 644000, People's Republic of China, Email 714170033@qq.com

Purpose: This study aims to develop a quercetin-loaded nanoparticles (QNP) with enhanced brain delivery capacity, which enables efficient delivery of quercetin to target brain regions under the guidance of borneol for the treatment of depression.

Methods: We prepared QNP via the thin-film dispersion method and characterized them by particle size, polydispersity index (PDI), zeta potential, morphology, release profile, and stability. Subsequently, a suite of models and assays including hemolysis test, cellular CCK-8 assay, cellular uptake experiment, and lipopolysaccharide (LPS) induced BV2 cell stress model were employed to comprehensively assess the antidepressant activity of QNP. Finally, we validated the in vivo antidepressant effect of QNP using an established depression mouse model.

Results: QNP exhibit a spheroidal shape with favorable particle size, PDI, and zeta potential. They have high encapsulation efficiency and exhibit sustained drug release capability. QNP remain stable in serum and saline solution. They maintain stability after 30 days of storage at room temperature. Results from the hemolysis test and cellular CCK-8 assay preliminarily suggested that QNP had a favorable safety profile. Additionally, cellular uptake experiments showed that the uptake rate of QNP by cells was nearly twice that of the quercetin. Assays using corticosterone- and hydrogen peroxide-induced PC12 cell injury models demonstrate that QNP exert a concentration-dependent cytoprotective effect. In the LPS-induced BV2 cell stress model, QNP exhibit superior inhibitory activity against NO and ROS compared with Qu. They also significantly inhibit IL-1β transcription. In vivo studies indicated that, compared with the first-line antidepressant fluoxetine, QNP alleviated depressive-like behaviors more effectively.

Conclusion: The lipid nanodrug delivery system QNP exhibit sustained drug release and enhanced cellular uptake. By virtue of safety and improved delivery efficiency, they multidimensionally augment the therapeutic efficacy of antidepressants. This is crucial for translating quercetin from a dietary supplement into a precision antidepressant.

Keywords: depression, quercetin, lipid nanoparticles, inflammation, oxidative stress

Introduction

Major depressive disorder (MDD) represents a globally significant public health concern, affecting over 300 million individuals worldwide and exacerbating the global disease burden.[1] Traditional antidepressants targeting the monoaminergic system are hindered by several drawbacks, including delayed onset of action, a high rate of non-response among patients, and a broad range of adverse effects.[2,3] Ketamine, a novel rapid-acting antidepressant capable of restoring neuroplasticity, can alleviate symptoms in patients with MDD within hours. However, its therapeutic effect typically persists for only a few days to one week, necessitating frequent injections for patients. This not only imposes a burden on patients but also increases the risk of drug dependence and adverse reactions.[4] These factors severely restrict the options

Received: 25 July 2025
Accepted: 16 December 2025
Published: 26 December 2025

Graphical Abstract

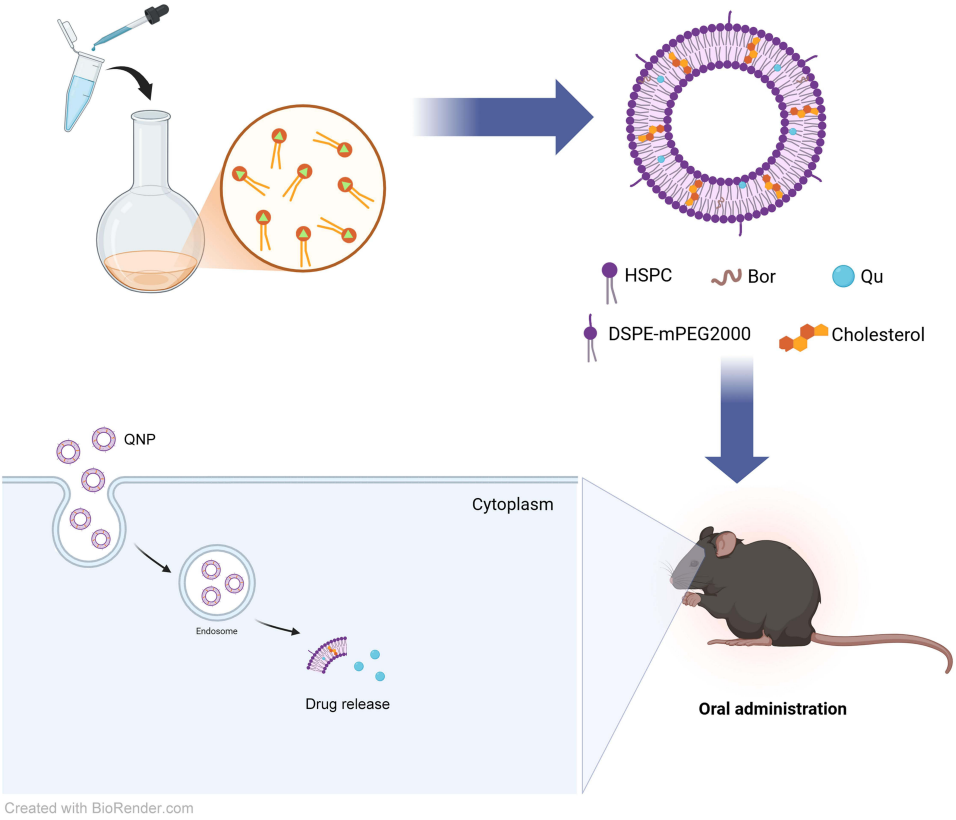

for pharmacotherapeutic interventions in MDD, thereby underscoring an urgent need to explore new therapeutic agents for MDD. Neuroinflammation is recognized as one of the key pathological underpinnings in the pathogenesis of depression, characterized by excessive activation of neuroglial cells—particularly microglia, which function as immune surveillance cells in the central nervous system (CNS).[5,6] Developing antidepressant therapeutic agents from a drug library that can modulate neuroinflammation and oxidative stress represents a highly promising strategy.[7–9]

Phytochemicals, widely distributed in foods and Chinese herbal medicines, have garnered substantial attention owing to their low toxicity, minimal side effects, and favorable antidepressant activity. Quercetin (Qu), a natural bioflavonoid abundant in various fruits and vegetables, has attracted significant interest due to its potent anti-inflammatory and antioxidant properties, which are thought to underpin its potential neuroprotective effects.[10–12] Qu contains hydroxyl groups in its structure, which facilitate electron donation to neutralize free radicals and inhibit the chain reaction of oxidative damage.[13] Moreover, Qu is a promising multi-target inhibitor of microglial activation, with the ability to protect neurons from microglia-mediated inflammatory toxicity.[14] Studies have demonstrated that Qu exerts a range of effects, including anti-inflammation, antioxidation, upregulation of brain-derived neurotrophic factor (BDNF) levels, elevation of serotonin (5-HT) levels, and attenuation of hypothalamic-pituitary-adrenal (HPA) axis hyperactivation.[11,15] These multiple mechanisms of action provide experimental support for the potential clinical application of Qu as an antidepressant. However, orally administered Qu undergoes extensive first-pass metabolism in the liver and intestines, which significantly reduces its systemic bioavailability; most of the drug is metabolized before exerting therapeutic effects.[16] This issue is particularly pronounced in long-term treatment, as it limits the sustained circulation of Qu at therapeutic concentrations. More critically, the highly selective barrier function of the blood-brain barrier (BBB) results in extremely low brain delivery efficiency of Qu (< 1%). Additionally, its poor aqueous solubility and insufficient

stability under physiological conditions further impede its BBB penetration, reduce its bioavailability, and significantly lower the effective drug concentration in the CNS—ultimately hindering the full manifestation of its neuroprotective efficacy.[17,18] Therefore, innovative strategies are required to enhance the delivery of Qu to the central nervous system for the treatment of MDD.

Recent advances in nanotechnology have provided a revolutionary solution to the inadequate brain delivery.[19,20] Nanotechnology-based drug delivery systems offer significant advantages for delivering hydrophobic drugs such as Qu, including high encapsulation efficiency, prolonged circulation time, controlled release, and enhanced therapeutic efficacy.[21,22] Furthermore, their small size results in a high surface-to-volume ratio, endowing them with unique physicochemical properties and biocompatibility. These features not only ensure stability and controlled release but also enhance mucosal adhesion.[23,24] Among various nano-delivery excipients, borneol (Bor)—a highly lipid-soluble bicyclic monoterpene—stands out as a promising brain-targeting auxiliary ligand.[25,26] With a clinical application history of over 1500 years in traditional Chinese medicine, Bor exerts effects such as inducing resuscitation, refreshing the mind, and exhibiting antipyretic and analgesic properties, particularly in the treatment of encephalopathies.[27] It can enhance the permeability of drugs across biological barriers, including the skin, nasal mucosa, and cornea. Mechanistically, Bor can bind to or adsorb onto cell membranes, alter membrane fluidity, promote the ordered arrangement of phospholipid molecules, and thereby facilitate transmembrane drug transport. Furthermore, it can enhance the transport and retention of macromolecules in the brain by increasing pinocytic vesicles. This effect is mediated through the regulation of various ATP-binding cassette transporters, inhibition of P-glycoprotein (P-gp) activity, upregulation of transmembrane tight junction proteins, and elevation of vasodilatory neurotransmitters.[28] These properties collectively render Bor a promising brain-targeting auxiliary ligand. Therefore, integrating borneol's barrier penetration-enhancing effect, non-invasive brain-targeting capability, and the controlled drug release advantages of nanocarriers for delivering Qu to specific brain regions is expected to open up a novel avenue for the effective treatment of brain diseases, particularly MDD.

Aiming to address the limitation that Qu exhibits poor bioavailability and inadequate targeting following administration, resulting in limited efficacy in treating depression, this study proposes a core hypothesis that the combination of lipid-based nano-delivery system and borneol modification to promote brain delivery may realize efficient brain delivery of Qu, and become an effective therapeutic agent for depression. Around this goal and hypothesis, this study designed and prepared the target preparation QNP, and systematically evaluated QNP through a series of experiments in vitro and in vivo, in order to provide a safe and targeted new path for improving the effectiveness of depression treatment.

Materials and Methods

Materials and Cell Lines

Qu (purity 99%) and Fluoxetine (Flu, purity 99%) was purchased from Macklin Biochemical Technology Co., Ltd. DSPE-mPEG2000, cholesterol, HSPC, borneol (Bor, purity 99%), dimethyl sulfoxide (DMSO), tetrahydrofuran, H_2O_2, corticosterone (CORT), and LPS were also obtained from Macklin Biochemical Technology Co., Ltd. DMEM high-glucose medium and fetal bovine serum were purchased from Gibco. Trypsin, Cyanine5.5 (Cy5.5) fluorescent dye, NO assay kit (S0021S), and DCFH-DA fluorescent probe kit (S0033S) were acquired from Beyotime Institute of Biotechnology. Both differentiated PC12 cells and BV2 cells were obtained from the Basic Medicine Laboratory of the Affiliated Hospital of Southwest Medical University (Sichuan, China). All other reagents used were of analytical grade and obtained from commercial sources.

Preparation of QNP

Accurately weigh 10 mg of Qu, 10 mg of Bor, 10 mg of cholesterol, 40 mg of HSPC, and 30 mg of DSPE-mPEG2000, and dissolve them in 5 mL of tetrahydrofuran in a 100 mL round-bottom flask. Under a constant-temperature water bath at 40 °C, stir the mixture at 100 rpm for 30 min. Subsequently, remove the tetrahydrofuran using a rotary evaporator via vacuum rotary evaporation at 40 °C and 100 rpm for 5 min, resulting in the formation of a lipid film on the inner wall of the flask. Purge with nitrogen to ensure no residual tetrahydrofuran remains, then place the flask in an oven at 60 °C for approximately 2 h. Following the addition of distilled water for hydration, disperse the nanoparticles uniformly using an

ultrasonic cell disruptor (160 W, 5 min) to obtain a clear QNP solution. For long-term storage of QNPs, pre-freeze the QNP solution in a −80 °C freezer, then lyophilize the product using a freeze dryer for approximately 24 h to yield a loose, yellowish-green QNP lyophilized powder. Blank NPs were prepared following the same protocol but without the addition of Qu.

Characterization of Morphology and Structure

For the determination of particle size, PDI (a parameter reflecting the uniformity of particle size distribution), and ζ potential of QNPs, the QNP solution was diluted to a concentration of 0.1 mg/mL, transferred to a 1 mL sample cell, and analyzed using a Malvern particle size analyzer (Zetasizer Nano S90, Malvern Panalytical) at 25 °C. The morphology of the samples was characterized using a low-voltage transmission electron microscope (TEM, Model JEM-1200EX; JEOL Ltd., Japan). Briefly, an aqueous sample solution was dropped onto a copper grid, negatively stained with 1% (w/v) sodium phosphotungstate, and then scanned via TEM to acquire morphological images.

Encapsulation Efficiency and Loading Efficiency of QNP

Accurately weigh 10 mg of QNP lyophilized powder and 10 mg of Qu raw material (as a reference), respectively. To completely release and dissolve the encapsulated Qu, 5 mL of methanol was added to each sample, followed by sonication for 4 min. After appropriate dilution, the QNP lipid nanoparticle solution and Qu raw material solution were obtained. Following centrifugation (8000 rpm, 10 min), the Qu content in each solution was determined by HPLC. The Qu concentration in the QNP solution was recorded as C1, and that in the Qu raw material solution as C2. The encapsulation efficiency (EE) was calculated using the formula:

$$\mathrm{EE}(\%) = (\mathrm{C1}/\mathrm{C2}) \times 100\%$$

For the determination of loading efficiency (LE), accurately weigh 10 mg of QNP lyophilized powder, designated as W, and fully dissolve it in 5 mL of pure water. To disrupt the lipid nanoparticles and release the encapsulated Qu, 5 mL of methanol was added, followed by sonication for 4 min. After dilution by 100 times and centrifugation (8000 rpm, 10 min), the Qu content was determined by HPLC. The actual amount of Qu in W (10 mg) of lyophilized powder, designated as W1, was calculated by substituting the measured value into a pre-established standard curve. The LE was calculated using the formula:

$$\mathrm{LE}(\%) = (\mathrm{W1}/\mathrm{W}) \times 100\%$$

Release Behavior and Stability of QNP

In vitro release studies were conducted via the dialysis method using an intelligent dissolution tester (ZRS-8G, Tianda Tianfa Technology Co., Ltd). A total volume of 120 mL PBS (Phosphate buffered saline) was used as the release medium to investigate the release profile of QNP. Since the free drug (Qu) is poorly water-soluble, a specified amount of surfactant (0.2% Tween 80) was added to the release medium.[29–32] A dialysis bag (molecular weight cutoff: 8000–14000 Da) was filled with 2 mL of QNP and 2 mL of free Qu, each at the same drug concentration (1 mg/mL). The release medium was maintained at 37 ± 0.5 °C under continuous stirring at 100 rpm. At predetermined time points (0 h, 0.25 h, 0.5 h, 1 h, 2 h, 4 h, 8 h, 12 h, and 24 h), 2 mL of dialysate was withdrawn and immediately replaced with an equal volume of fresh release medium to maintain a constant total volume. Following centrifugation of the dialysate, the concentration of Qu was determined using UV-visible spectroscopy. All samples were analyzed in triplicate via UV-visible spectroscopy for each in vitro release experiment. The cumulative release percentage at each time point was calculated using the standard curve, and the in vitro release profile was constructed. Finally, the release behavior of each drug group was fitted to kinetic models (zero-order release equation, first-order release equation, and Higuchi equation) based on the release profiles and corresponding data.

For the serum stability study, a QNP stock solution (0.1 mg/mL) was prepared with ultrapure water as solvent. The stock solution was mixed with fetal bovine serum (FBS) at a 1:1 volume ratio, yielding a final FBS concentration of 50% to simulate the in vivo blood environment. The mixed samples were placed in a constant temperature shaker at 37°C with

a rotation speed of 100 rpm and incubated for 2 h prior to the determination of particle size and PDI values. For the salt stability study, 0.9% NaCl (a physiologically relevant concentration) was used. Equal volumes (100 μL each) of QNP stock solution and normal saline were mixed. The mixture was transferred to a constant temperature shaker at 37 °C, maintained at 100 rpm, and incubated for 2 h. Particle size and PDI values were then measured. Additionally, the changes in particle size and PDI of QNP were monitored over a one-month storage period at room temperature.

Hemolytic Analysis

To evaluate the biological safety of liposomes during blood circulation, a hemolysis assay was performed. Fresh blood was collected from the retro-orbital sinus of mice and transferred to test tubes containing an anticoagulant. Fibrinogen was removed by gentle clockwise stirring with a glass rod for 5 min. 2.5 mL of 0.9% sodium chloride solution was added, followed by stirring and centrifugation at 1500 rpm for 10 min, the supernatant was then discarded. To isolate red blood cells (RBCs), 0.9% sodium chloride solution was added again, and the above washing and centrifugation steps were repeated until the supernatant was colorless. A 2% RBC suspension was prepared by resuspending the cells in 0.9% sodium chloride solution. QNP samples (at concentrations of 50, 100, 150, and 200 μg/mL), along with a negative control (normal saline) and a positive control (ultrapure water), were incubated in a 37 °C incubator for the hemolysis assay. After 5 h of incubation, all samples were centrifuged at 1500 rpm for 10 min to assess hemolysis. The supernatant of each sample was transferred to a 96-well plate, and absorbance (A) was measured at 540 nm using a microplate reader. The hemolysis rate (%) was subsequently calculated.

Cytotoxicity Evaluation

The effect of QNP at gradient concentrations on the viability of PC12 and BV2 cells was evaluated using the CCK-8 assay, respectively. Cells were resuscitated in DMEM high-glucose medium supplemented with 10% fetal bovine serum (FBS) and maintained in a cell incubator at 37°C with 5% CO_2. When cells reached the logarithmic growth phase, they were seeded into 96-well plates at a density of approximately 5000 cells per well. After the cells had adhered and incubated for 24 h, 100 μL of QNP solution at each gradient concentration (10, 7.5, 5, 2.5, and 1 μg/mL) was added to the corresponding wells. For the blank group, an equal volume of blank medium was added. Following 24 h of incubation, CCK-8 reagent was added, and incubation was continued for another 4 h. Cell viability was then measured using a microplate reader. The formula for calculating the cell proliferation rate is:

$$\text{Cell proliferation rate}(\%) = \left[\frac{A_{\text{Experimental group}} - A_{\text{Blank group}}}{A_{\text{Control group}} - A_{\text{Blank group}}}\right] \times 100\%$$

Cell Uptake

Fluorescence microscopy was employed to assess the cellular uptake of QNP. Fluorescent labeling serves as a practical approach for detecting compounds with suboptimal spectral properties. Specifically, fluorescently labeled liposomes were prepared by incorporating Cy5.5 (as a fluorescent tracer) into the liposome formulation. BV2 cells in the logarithmic growth phase were seeded into 6-well plates at a density of 3×10^5 cells/well and allowed to adhere and culture for 24 h. Three groups were established: a blank control group, QNP groups with gradient concentrations (fluorescently labeled with Cy5.5), and Qu groups with corresponding gradient concentrations. For the blank control group, 100 μL of culture medium was added; whereas, for the administration groups, 100 μL of culture medium containing the respective drugs at concentrations of 1, 5, and 10 μg/mL was added. After incubation for 2 h and 4 h, the culture medium was aspirated, and BV2 cells were washed three times with PBS (pH 7.4) to remove residual drugs, followed by fixation with 4% paraformaldehyde for 20 min. Subsequently, extracellular residual staining solution was removed by extensive washing with pre-cooled PBS. Samples were visualized under an inverted fluorescence microscope, and images were captured using the Olympus UC90 color imaging system.

To quantify the cellular uptake efficiency of QNP, high-performance liquid chromatography (HPLC) was employed for quantitative analysis. BV2 cells were seeded in 6-well plates and allowed to adhere for 24 h before being treated with QNP for 4 h. Following treatment, cells were detached using cell scrapers and centrifuged at 800 rpm for 5 min. The cell

pellet was resuspended in ice-cold cell lysis buffer supplemented with a protease inhibitor cocktail and incubated on ice for 30 min to ensure complete lysis. Subsequently, proteins were precipitated by adding four volumes of methanol to the lysate, followed by centrifugation at high speed to isolate QNP. The resulting supernatant was then analyzed via HPLC for quantification. The cell uptake rate is calculated as follows:

$$\text{Cell uptake rate}(\%) = \left[\frac{\text{Concentration of intracellular QNP} * \text{Volume of the, supernatant}}{\text{Total amount of QNP initially added}}\right] \times 100\%$$

Evaluation of Corticosterone-Induced PC12 Cell Injury Model

PC12 cells in the logarithmic growth phase were seeded into 96-well plates. Following adherence and incubation for 24 h, the following groups were established: a blank control group, a corticosterone model group, QNP groups with gradient concentrations, and Qu groups with corresponding gradient concentrations. For the blank control group, 100 μL of blank complete medium was added. For the corticosterone model group, 100 μL of complete medium containing corticosterone was added. For the administration groups, 100 μL of complete medium containing the respective drug (at concentrations of 1, 5, and 10 μg/mL) in combination with corticosterone was added. After 24 h of incubation, CCK-8 reagent was added, followed by an additional 4 h of incubation. Subsequently, cell viability was measured using a microplate reader, and the relative cell proliferation rate was calculated using the formula described in Cytotoxicity Evaluation.

Evaluation of H_2O_2-Induced PC12 Cell Injury Model

PC12 cells in the logarithmic growth phase were seeded into 96-well plates. Following adherence and incubation for 24 h, the following groups were established: a blank control group, an H_2O_2 model group, QNP groups with gradient concentrations, and Qu groups with corresponding gradient concentrations. For the blank control group, 100 μL of blank complete medium was added. For the H_2O_2 model group, 100 μL of complete medium containing H_2O_2 was added. For the administration groups, 100 μL of complete medium containing the respective drug (at concentrations of 1, 5, and 10 μg/mL) in combination with H_2O_2 was added. After 24 h of incubation, CCK-8 reagent was added, followed by an additional 4 h of incubation. Cell viability was then measured using a microplate reader, and the relative cell proliferation rate was calculated using the formula described in Cytotoxicity Evaluation.

Evaluation of Inhibitory Effect on NO Release and Interleukin-1β Transcription

BV2 cells in the logarithmic growth phase were seeded into 96-well plates and incubated for 24 h to allow for cell adherence. The original medium was then replaced with high-glucose medium containing QNP or Qu at three concentrations (low: 1 μg/mL, medium: 5 μg/mL, high: 10 μg/mL) in combination with LPS. Each treatment group was set up in triplicate. Following 12 h of intervention, the culture supernatant was collected by centrifugation, and the NO content was measured using a commercial NO detection kit according to the manufacturer's instructions. Briefly, the NO assay reagent was added to the supernatant, and after the reaction was complete, the absorbance was measured using a microplate reader. The relative NO content of each group was then calculated.

To determine the expression of proinflammatory cytokine mRNAs such as IL-1β, total RNA was extracted from cells following intervention in each group. Reverse transcription of the extracted total RNA was performed using a Takara reverse transcription kit in a total reaction volume of 20 μL. Subsequently, amplification of the products was performed following Takara's qPCR protocol. Relative mRNA expression levels of target genes were calculated using the 2-ΔΔCt method with GAPDH as the internal control. Detailed primer information is provided in Table 1.

Table 1 List of Primers Used for qRT-PCR

Gene	Species	Forward Sequence (5′–3′)	Reverse Sequence (5′–3′)
IL-1β	Mouse	GTGTCTTTCCCGTGGACCTTC	TCATCTCGGAGCCTGTAGTGC
GAPDH	Mouse	GACATCAAGAAGGTGGTGAAGC	GAAGGTGGAAGAGTGGGAGTT

Evaluation of the Inhibitory Effect on ROS Release

BV2 cells in the logarithmic growth phase were seeded into 24-well plates and incubated for 24 h to allow adherence. The original medium was then replaced with high-glucose medium containing QNP or Qu at three concentrations (low: 1 μg/mL, medium: 5 μg/mL, high: 10 μg/mL) in combination with LPS, with each group set up in triplicate. After 12 h of intervention, the culture supernatant was discarded, and cells were washed three times with PBS. Reactive oxygen species (ROS) assay reagent was then added according to the manufacturer's instructions for the ROS detection kit. Following the reaction, staining was visualized under an inverted fluorescence microscope, and fluorescence intensity in each group was measured using a microplate reader. Finally, the relative ROS fluorescence intensity in each group was calculated, with results expressed as relative fluorescence intensity (where the blank control group was set as 100%).

In vivo Antidepressant Effect of QNP

To establish the chronic unpredictable mild stress (CUMS) model of MDD, we used male C57BL/6J mice. These mice were aged 4 weeks and weighing 18 ± 2 g, which were obtained from Chongqing Tengxin Science and Technology Experimental Animal Co., Ltd. All mice were housed in a clean environment under a stable 12 h light/dark cycle. Ambient temperature was maintained at 25 ± 2°C, and relative humidity was controlled at 40–60%. All animal experiments were approved by the Ethics Committee of Chongqing University Central Hospital (NO.2502002).

After newly purchased mice were acclimated to the environment for 1 week, they were randomly divided into two groups: the blank control group and the CUMS model group. Mice in the blank control group were housed under normal conditions, while those in the model group received unpredictable behavioral stimuli 1 to 2 times per day. The stimuli included 24 h food deprivation, 2 h noise stimulation, 10 min of vigorous cage shaking, 5 min of ice water swimming, 5 min of hot water swimming, 8 min of upside-down hanging, 1 h of restraint in a 50 mL centrifuge tube, 2 min of mild electric shock, 48 h of continuous light, and 48 h of continuous darkness. The same stimulus type was not applied on consecutive days, and model establishment lasted for 42 days.

Following successful CUMS model establishment, 6 mice remained in the blank control group. Additionally, mice that exhibited depressive-like behaviors were further divided into 4 subgroups with 6 mice each, including the CUMS group, the Flu group, the low-dose QNP group, and the high-dose QNP group. Mice in the Flu group were oral administered 10 mg/kg Flu. Mice in the low-dose and high-dose QNP groups received 10 mg/kg and 50 mg/kg QNP, respectively.[33,34] Mice in the blank control and CUMS groups were given an equal volume of normal saline. All treatments were administered once daily for 28 consecutive days. Following the 28-day treatment period, the open field test, forced swimming test, and sucrose preference test were performed to evaluate depressive-like behaviors.

Statistical Analysis

All data were analyzed with GraphPad Prism 10.1.2 software. Data are expressed as mean ± standard deviation (SD) based on three independent biological replicates. Prior to formal statistical analysis, data normality was assessed via the Shapiro–Wilk test and variance homogeneity was evaluated using Levene's test. For comparisons between two groups, the Student's *t*-test was used when data met normality and variance homogeneity. For comparisons among multiple groups, one-way analysis of variance (ANOVA) was initially applied. Tukey's honest significant difference (HSD) test was then used for post-hoc analysis. This post-hoc test inherently includes multiple comparison correction to control Type I error. Statistical significance was defined as $P < 0.05$.

Results and Discussion

Results of Physicochemical Characterization of QNP

As shown in Figure 1, by optimizing the preparation process of lipid nanoparticles, the final light yellowish-green product, QNP, was obtained (Figure 1A). Liposome stability can be enhanced via surface modification with polyethylene glycol (PEG). Additionally, PEG prolongs the drug's half-life in the bloodstream by reducing interactions between liposome-encapsulated drugs and serum proteins. The particle size, PDI, and Zeta potential were measured using a Malvern particle size analyzer, with the results shown in Figure 1B and C. After reconstitution of the lyophilized

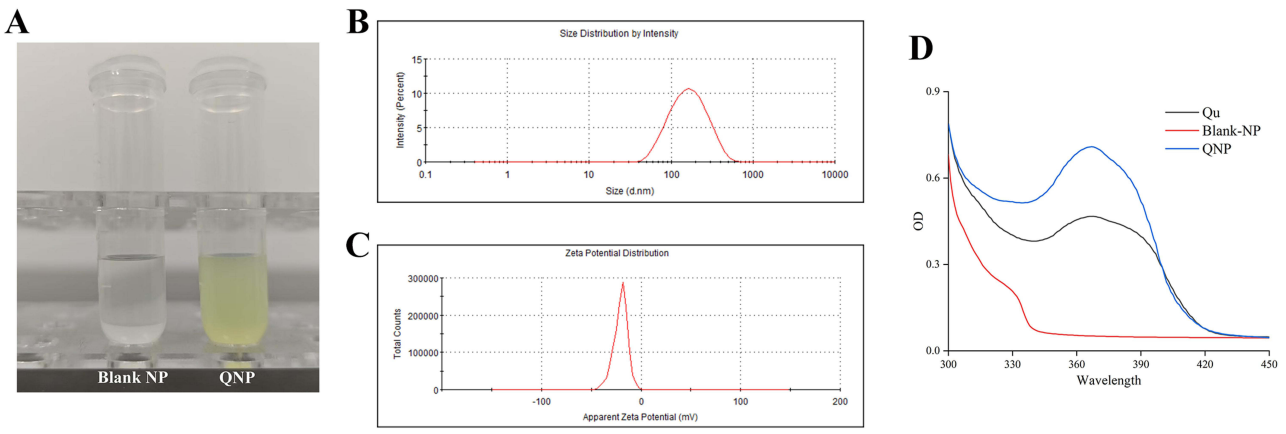

Figure 1 Characterization results of QNP. (**A**) Digital images of blank nano liposomes and QNP liposomes. (**B**) Particle size distribution profile of QNP as determined by a Malvern particle size analyzer. (**C**) Zeta potential profile of QNP as determined by a Malvern particle size analyzer. (**D**) UV scanning spectra of Qu, blank nano liposomes, and QNP. ($\bar{x}$ ± s, n = 3).

formulation, the average particle size was determined to be 133 nm, the PDI was 0.249, and the Zeta potential was −20.5 mV. The above results indicate that the lipid nanoparticles have an appropriate particle size. A PDI of 0.249 (< 0.3) suggests uniform dispersion of the particles, while a Zeta potential of −20.5 mV indicates that the particles are overall negatively charged. The Zeta potential of nanoparticles is an important physicochemical parameter, as it determines the strength of interparticle interactions and the adsorption of counterions, thereby governing the stability of the particles. Zeta potential describes the charge distribution of bare particles associated with the diffuse layer.[35] A high Zeta potential, either positive or negative, implies strong electrostatic repulsion between particles, which enhances stability. Generally, a Zeta potential with an absolute value exceeding 30 mV indicates an electrostatically stable system. Limited flocculation or short-term stability can be observed between 5 and 30 mV, while a Zeta potential below 5 mV typically leads to particle aggregation. For dispersions stabilized by a combination of steric and electrostatic effects, a Zeta potential of approximately 20 mV is ideal. However, for better long-term storage, preparation as a lyophilized powder is a more optimal choice. UV scanning results for Qu raw material, blank formulation, and QNP are presented in Figure 1D. Both Qu and QNP exhibit maximum UV absorption at 367 nm, whereas the blank formulation shows no characteristic absorption at this wavelength. This indicates that the formulation excipients and Bor do not interfere with the UV absorption of Qu. Moreover, in subsequent HPLC analyses, the established HPLC method for Qu can be directly applied to quantify Qu in QNP. EE and LE of the optimized QNP were determined, revealing that QNP possesses acceptable drug loading capacity, with an EE of 78.35 ± 3.65% and a LE of 6.65 ± 0.13%. TEM was employed to characterize the morphology of QNP to enable more intuitive observation. As shown in the TEM images (Figure 2A), QNP exhibit a spherical morphology and uniform size distribution. HSPC is widely acknowledged to undergo spontaneous self-assembly in aqueous environments. This process is synergistically regulated by hydrophobic and hydrophilic interactions. Among these interactions the hydrophobic effect serves as the core driving force for lipid self-assembly. It facilitates the formation of ordered structural arrangements to minimize the interactions between hydrophobic hydrocarbon chains and the surrounding aqueous phase. Thus following successful preparation most liposomes exhibit a spherical morphology.

Results of Drug Release Behavior and Stability of QNP

An optimal drug release rate is critical in clinical practice. Incorporating drugs into lipids not only imparts stability to the formulation but also enables sustained release, thereby enhancing the overall efficacy of the drug delivery system. Investigating in vitro release to predict in vivo pharmacokinetics of formulations reduces the burden of in vivo studies during drug development. The dialysis method is widely used to simulate in vitro release kinetics of nanoparticle-based drug delivery systems. Here, the release rate of Qu from QNP was measured using PBS (pH 7.4) as the release medium at 37 °C and compared with that of free Qu. The results are presented in Figure 2B and C. Qu exhibited a rapid release profile, with 80.20 ± 3.19% released within 4 h. In contrast, QNP displayed a biphasic release pattern: an initial burst

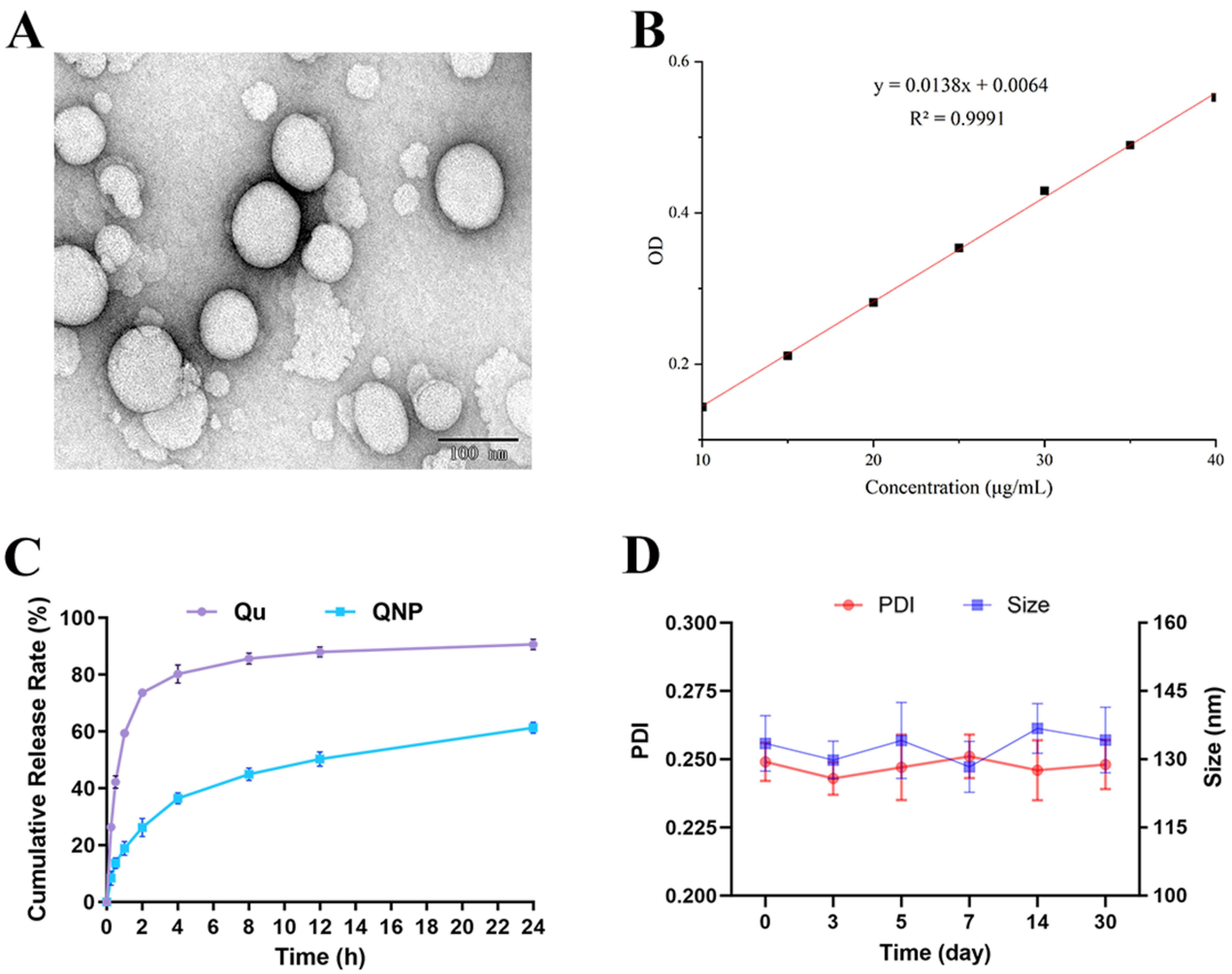

Figure 2 In vitro release behavior of QNP. (**A**) TEM image of QNP acquired using a transmission electron microscope. (**B**) Solubility standard curve of Qu. (**C**) Release profiles of Qu and QNP in PBS release medium (pH 7.4) over 24 h. (**D**) Particle size and PDI changes of QNP during 30 days of room temperature storage.

release followed by a sustained release phase. Specifically, 36.45 ± 1.93% of the drug was released rapidly within 4 h, and the cumulative release reached 62.33 ± 1.97% by 24 h. Notably, equilibrium was not achieved during the entire process, with a continuous release trend still observed after 24 h. Based on the fitted data from in vitro release studies, as shown in Table 2, the bulk drug Qu adheres to the first-order kinetic model, while QNP exhibits a better fit to the Higuchi model. Consistent with the release behavior of liposomes, nanoliposomal drug release occurs in two stages: initially, drug diffuses from the lipid matrix, and subsequently, as the lipid degrades, drug entrapped within the membrane is slowly released. This result highlights the capacity of liposomes to enable sustained Qu release from QNP.

Stability evaluation of QNP was subsequently conducted. In serum solution, QNP exhibited a particle size of 136.82 ± 4.72 nm and a PDI of 0.252 ± 0.008. Similarly, in normal saline, QNP showed a particle size of 133.26 ± 6.15 nm and a PDI of 0.248 ± 0.010. These findings demonstrate that QNP maintains good stability in both serum and normal saline. Additionally, the room-temperature stability of QNP lyophilized powder was assessed, with the results presented in

Table 2 Fitting Coefficients of Qu and QNP in Different Release Models

Drug	Zero-Order Release Model	First-Order Release Model	Higuchi Model
Qu	−1.035	0.890	0.313
QNP	0.134	0.581	0.908

https://doi.org/10.2147/IJN.S556128

Figure 2D. Over a 30-day storage period at room temperature, no significant changes were observed in the particle size or PDI of QNP. This indicates that QNP lyophilized powder can be stably stored at room temperature for a minimum of 30 days.

Results of Hemolysis Experiment

Following in vivo absorption, nanomedicines may interact with body cells, potentially inducing severe hemolysis. Therefore, in vitro hemolysis assays are commonly used to preliminarily evaluate drug biocompatibility and predict their potential to induce in vivo hemolysis. A nanomedicine is considered to have good hemocompatibility when its hemolysis rate is below 5%. As shown in the Figure 3A and B, in the negative control group of this study, no hemolysis was observed in cells following the addition of normal saline. In the positive control group, upon addition of ultrapure water, cells rapidly underwent hemolysis, exhibiting a bright red appearance with a hemolysis rate of 100%. For QNP, the hemolysis rate was well below 5% across the concentration range of 50–200 μg/mL. Specifically, at the maximum QNP concentration of 200 μg/mL, the hemolysis rate was only 0.16 ± 0.60%. This indicates that QNP exhibit good hemocompatibility within this concentration range.

Results of Cytotoxicity Experiment

To preliminarily evaluate the cytotoxicity of QNP on central nervous system cells and screen out a suitable concentration range for administration, cytotoxicity assays were performed using PC12 and BV2 cells. The selection of the initial drug concentration drew on previous studies and was appropriately optimized based on results from the early-stage preliminary experiments of this study.[36] The CCK-8 assay is widely used to assess cell viability and toxicity, based on the correlation between mitochondrial dehydrogenase activity and cell viability: higher cell viability corresponds to greater absorbance at a specific wavelength. Changes in absorbance thus indirectly reflect cell viability and the extent of toxic effects. Figure 4A shows the effect of QNP at different concentrations on PC12 cell viability. Within the concentration range of 1–10 μg/mL, PC12 cell viability was largely unaffected by QNP treatment, with no statistically significant differences in cell proliferation rates between groups ($P > 0.05$). Similarly, as shown in Figure 4B, BV2 cells grew well following QNP administration, with no significant differences in cell morphology or density between groups ($P > 0.05$). CCK-8 results also indicated that within 1–10 μg/mL, there were no statistically significant differences in cell proliferation rates between groups ($P > 0.05$). Cytotoxicity assay results provide a critical basis for selecting subsequent administration concentrations. In summary, preliminary screening indicates that QNP at concentrations of 1–10 μg/mL exhibit a favorable safety profile.

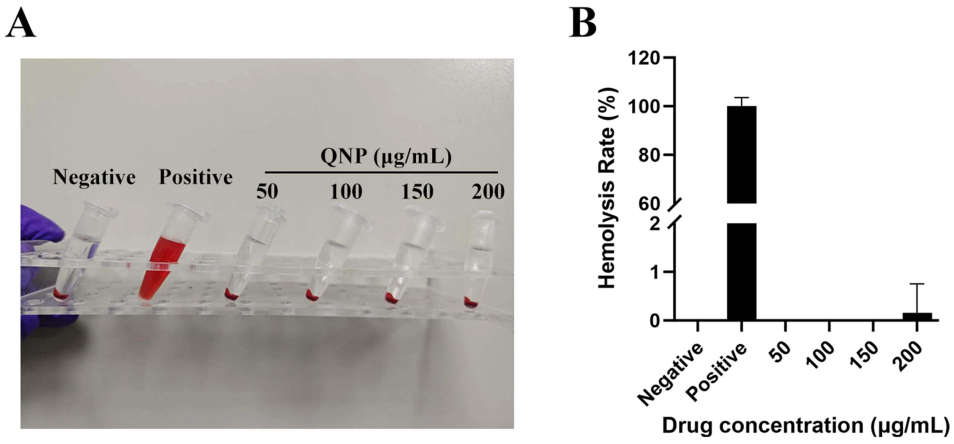

Figure 3 Hemolysis assay results of QNP. (**A**) Digital images of the QNP hemolysis assay at gradient concentrations. (**B**) Quantitative results of the QNP hemolysis assay. ($\bar{x}$ ± s, n = 3).

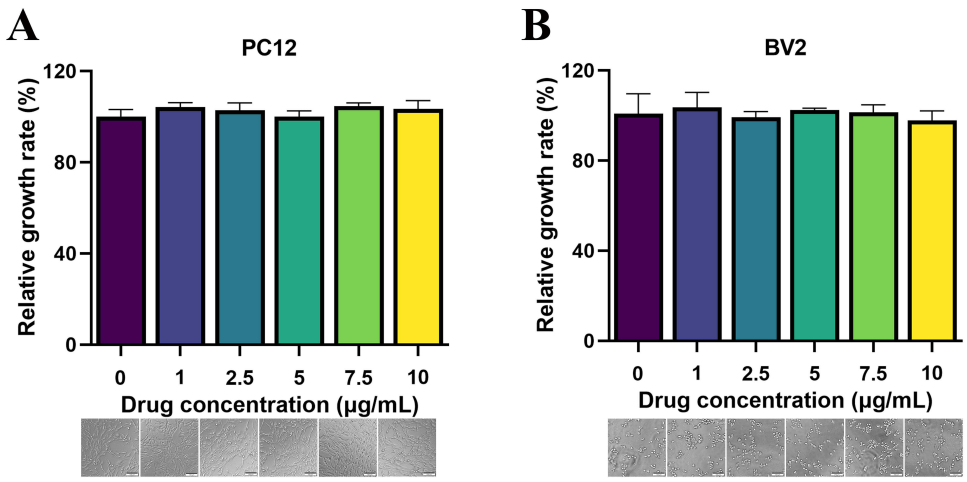

Figure 4 Cytotoxicity assay results of QNP. (**A**) Effects of QNP at gradient concentrations on the relative growth rate of PC12 cells, and digital images of representative cells at each concentration. (**B**) Effects of QNP at gradient concentrations on the relative growth rate of BV2 cells, and digital images of representative cells at each concentration. ($\bar{x}$ ± s, n = 3).

Results of Cell Uptake

Microglia play a key role in regulating inflammation within the CNS. Enhancing microglial uptake efficiency can effectively improve drug therapeutic efficacy. To verify whether QNP exhibit enhanced internalization by microglia, BV2 cells were used to assess the uptake rates of free Qu and QNP. Qualitative observation of Cy5.5-labeled nanoparticle internalization by BV2 cells was performed via fluorescence microscopy. As shown in the Figure 5A and B,

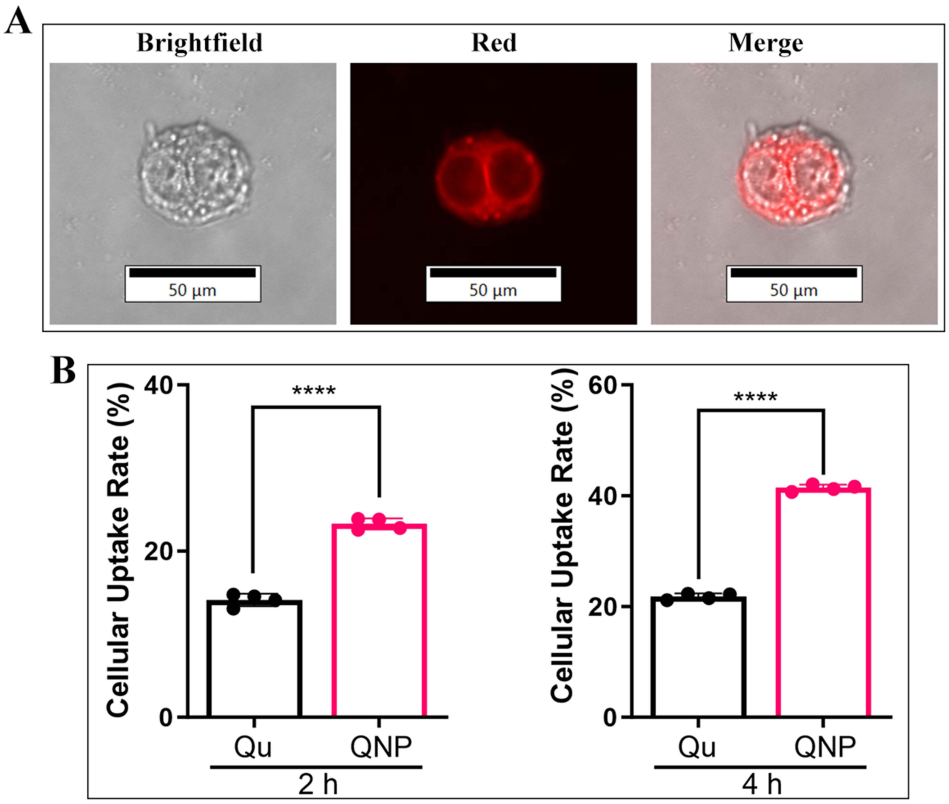

Figure 5 Results of the BV2 cell uptake rate assay for QNP. (**A**) Digital images of QNP uptake by BV2 cells. (**B**) Experimental results for the quantitative uptake of QNP. ****P < 0.0001. * indicate the significance between Qu group and QNP group. ($\bar{x}$ ± s, n = 4).

https://doi.org/10.2147/IJN.S556128

Cy5.5-labeled QNP emitted red fluorescence, with the drug predominantly localized in the cytoplasm following cellular entry. Quantitative uptake was measured via HPLC, and the figures illustrates time-dependent cellular uptake at 37 °C. At both 2 h and 4 h time points, QNP uptake by BV2 cells was higher than that of free Qu. Furthermore, uptake increased with longer co-incubation times, indicating time-dependent uptake in both groups and that liposomal encapsulation effectively enhances cellular drug uptake. It has been reported that endocytosis of Bor-modified nanoparticles is associated with the Golgi-mediated pathway and energy-dependent active transport.[37] Additionally, the ability of lipid membrane components (HSPC, cholesterol, and DSPE-mPEG2000) to promote cellular uptake involves other mechanisms, including downregulating the expression of ATP-binding cassette (ABC) transporters and enhancing membrane phospholipid fluidity.

Evaluation Results of CORT-Induced PC12 Cell Injury Model

Patients with depression frequently exhibit elevated serum cortisol levels. Common animal models used in depression research—including restraint stress, psychosocial stress, and predator odor exposure models—consistently elevate circulating CORT levels. Exposing mice to a high CORT environment induces depressive-like behaviors and downregulates the expression of BDNF in neurons of the hippocampal dentate gyrus. Moreover, a high CORT environment markedly inhibits the proliferation of neural stem cells, neural progenitor cells, and mature neurons; reduces the dendritic branching complexity and spine density of hippocampal granular neurons; and impairs the survival and migration of both newly generated immature neurons and mature neurons in the dentate gyrus (DG).[38,39] Following antidepressant treatment, these abnormalities can be effectively reversed. In the present study, PC12 cells were co-cultured with QNP at concentrations of 1, 5, and 10 μg/mL in the presence of CORT for 24 hours; the control group received treatment with Qu at the same concentrations, with results presented in the Figure 6A. The CORT-induced injury model reduced the relative proliferation rate of PC12 cells to 41.19 ± 0.52%. Following QNP treatment, a concentration-dependent cytoprotective effect was observed: at the highest concentration (10 μg/mL), the cell proliferation rate was significantly increased to 85.18 ± 0.58% ($P < 0.0001$). Although the Qu control group also exerted a concentration-dependent cytoprotective effect, at the maximum concentration of 10 μg/mL, it elevated the cell proliferation rate only to 75.00 ± 0.37%—a level comparable to that of the QNP group at 5 μg/mL. Consistent with previous studies, long-term treatment with clinically effective antidepressants may counteract corticosterone-induced effects by promoting the generation of new cells, or via corticosterone-independent mechanisms—such as upregulating growth factor levels in the hippocampus or modulating pro-apoptotic and anti-apoptotic factors—to attenuate such cell death.[40,41] In the present study, Qu exerted a favorable cytoprotective effect against CORT-induced damage, and this protective effect was further enhanced after Qu was successfully formulated into QNP lipid nanoparticles. Based on findings from drug release profile analyses and cellular uptake experiments, this enhanced efficacy may be attributed to the increased cellular uptake rate mediated by the successfully developed drug-loaded delivery system.

Evaluation Results of H_2O_2-Induced PC12 Cell Injury Model

Oxidative stress is defined as a pathological state where the levels of oxidants—such as hydrogen peroxide (H_2O_2), superoxide anion, and nitric oxide (NO)—exceed the antioxidant defense capacity of cells. These oxidants can modify intracellular macromolecules (eg, proteins, DNA, and lipids), thereby altering cellular functions and ultimately resulting in cell death.[42] Accumulating evidence has confirmed that patients with depression exhibit elevated levels of malondialdehyde (MDA) and H_2O_2, accompanied by increased DNA damage.[43,44] As a potent oxidant, H_2O_2 is electrically neutral, enabling it to traverse biological membranes; it plays a key role in growth factor-induced signal transduction, maintenance of thiol redox homeostasis, and regulation of mitochondrial function.[45,46] Upon induction with a high-dose H_2O_2, PC12 cells undergo stress-induced cell death.[47,48] To assess whether QNP exhibits comparable or superior cytoprotective efficacy to Qu, the optimal H_2O_2 concentration for inducing PC12 cell death was first determined. Subsequently, PC12 cells were co-cultured with QNP or Qu, and the cell proliferation rate following treatment was measured. Results are presented in the Figure 6B. After H_2O_2 induction, the relative proliferation rate of cells in the model group decreased to 44.14 ± 0.55%. Following co-culture with QNP, the relative cell viability increased in a concentration-dependent manner, with the proliferation rate significantly elevated to 75.31 ± 1.77% at the 10 μg/mL dose ($P < 0.0001$). At the same

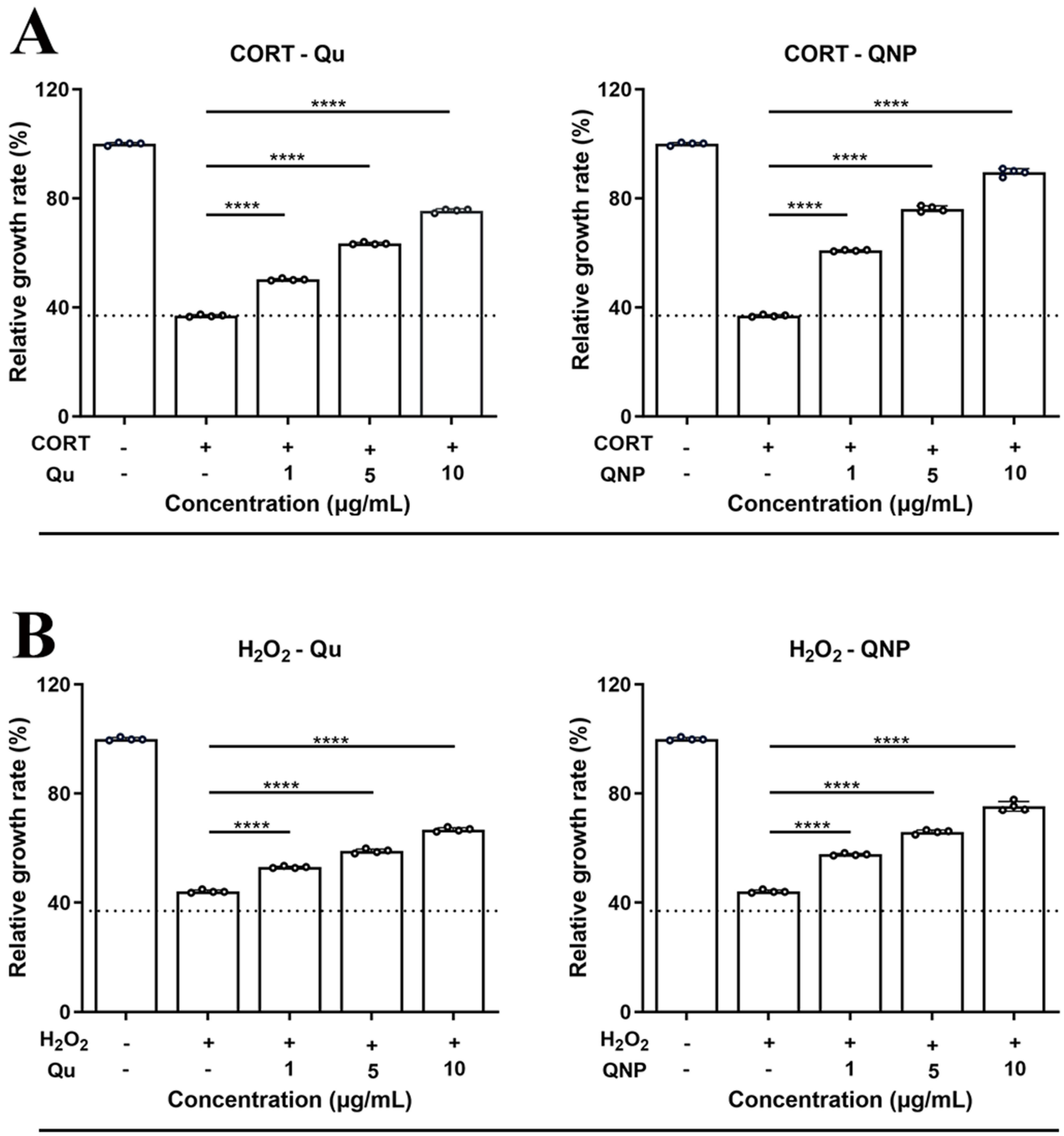

Figure 6 Results of the assay for the viability recovery effect of Qu and QNP at gradient concentrations on BV2 cells. (**A**) Viability recovery effect of Qu and QNP at gradient concentrations on BV2 cells after injury induced by CORT. (**B**) Viability recovery effect of Qu and QNP at gradient concentrations on BV2 cells after injury induced by H_2O_2. ****$P < 0.0001$. * indicates the significance between the drug group and the model group at a specific concentration. ($\bar{x} \pm s$, n = 4).

concentration, the Qu group only increased the proliferation rate to 66.82 ± 0.71%. These findings indicate that QNP also demonstrates greater efficacy than Qu in the H_2O_2-induced PC12 cell injury model.

Evaluation Results of Inhibitory Effect on NO Release and IL-1β Transcription

Microglia, the resident immune cells of the CNS with macrophage-like properties, become activated upon exposure to brain injury, neurotoxic stimuli, or inflammatory signals.[49] This activation prompts the release of various neurotoxic

https://doi.org/10.2147/IJN.S556128

mediators, including NO, IL-1β and other pro-inflammatory cytokines. In states of neuroinflammation, overproduced NO not only directly induces oxidative damage but also disrupts the dynamic balance between oxidative stress and antioxidant systems, thereby exacerbating neuronal dysfunction.[50] Notably, the pro-inflammatory agent LPS can concentration-dependently enhance nitric oxide synthase protein expression and NO release in BV-2 murine microglia, further supporting the critical role of the microglia-NO axis in underpinning the pathological mechanisms of depression.

Previous studies have indicated that Qu exerts potential in alleviating depression by regulating NO levels.[51,52] Therefore, in this study, LPS was used to induce BV2 cells to produce significant levels of NO and IL-1β. By comparing changes in biological effects following QNP or Qu intervention, we aimed to determine whether QNP exerted a protective effect. The results are shown in the Figure 7A. Compared with the blank control group, NO release in the LPS-induced model group increased by approximately 3.2-fold. Qu intervention resulted in a concentration-dependent reduction in NO release; at a Qu concentration of 10 μg/mL, NO release decreased to approximately 1.7-fold. In contrast, the QNP group exhibited lower NO release than the Qu group at all tested concentrations, with NO release reduced to approximately 1.3-fold at the maximum concentration. Figure 7B depicts the changes in IL-1β following QNP intervention. With increasing drug concentration, the transcription level of IL-1β was significantly inhibited ($P < 0.0001$). As a retrograde neurotransmitter, NO can rapidly diffuse to adjacent neurons to modulate their activity and diffuse back to presynaptic neurons to regulate the release of other neurotransmitters. Through these mechanisms, NO influences synaptic plasticity and synaptic strength. However, prolonged exposure to high NO concentrations may induce neuronal damage.[53] The results demonstrate that the QNP group outperforms the corresponding Qu group in reducing NO content and inhibiting IL-1β transcription, which contributes to neuroprotection and the regulation of neuronal plasticity.

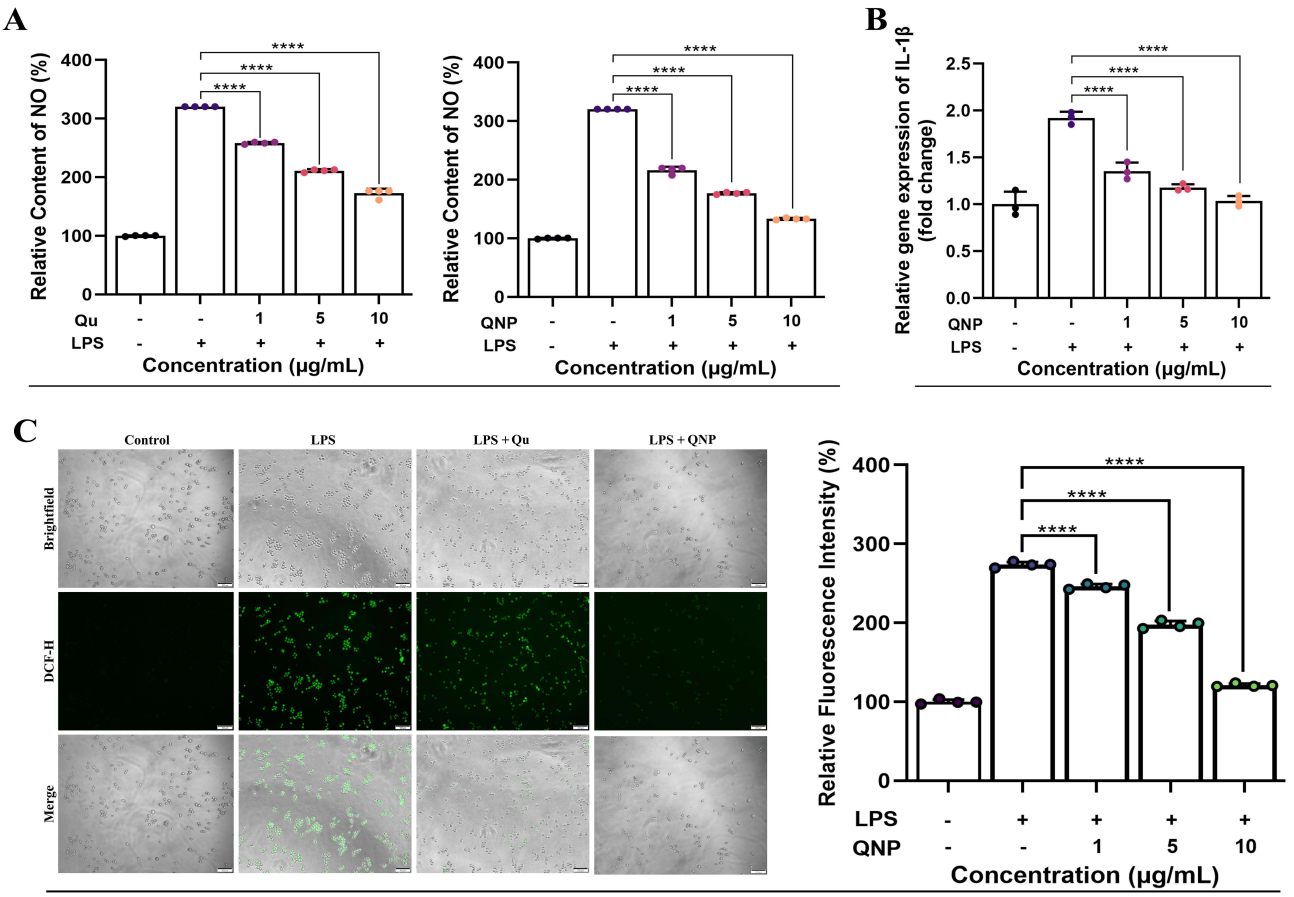

Figure 7 QNP inhibits LPS-induced microglial cytotoxic substances release. (**A**) Inhibition of NO release from BV2 cells by Qu and QNP at gradient concentrations after stress induction by LPS. (**B**) Inhibition of IL-1β transcription from BV2 cells by QNP after stress induction by LPS. (**C**) Inhibition of ROS release from BV2 cells by Qu and QNP at gradient concentrations after stress induction by LPS. ****$P < 0.0001$. * indicates the significance between the drug group and the model group at a specific concentration.

Evaluation Results of Inhibiting ROS Release

ROS participate in both pathological processes and physiological cellular signaling in organisms. Oxidative stress represents a state of cellular imbalance in which ROS production surpasses antioxidant defense mechanisms, mediating oxidative damage to DNA, RNA, and lipids and triggering diverse pathophysiological consequences. Previous studies have demonstrated that Qu can restore the expression of the pCREB/BDNF/PSD95/Synapsin1 signaling pathway in LPS-damaged hippocampi and decrease serum levels of inflammation-related factors.[54] Furthermore, Qu administration can alleviate the rapid elevation of ROS levels induced by LPS-triggered inflammatory storms and subsequent oxidative stress.[55] As depicted in the Figure 7C, LPS-induced modeling of BV2 cells in this study resulted in a significant increase in ROS levels ($P < 0.0001$). Consistent with the trend of NO release, ROS levels decreased in a concentration-dependent manner as the QNP administration concentration increased. Notably, at the same concentration, the QNP group exerted stronger biological effects compared to the Qu group. The oxidative stress pathway may drive the pathogenesis of depression through crosstalk with processes including neurogenesis, neuroplasticity, and neuroinflammation. Here, the superior ROS-inhibiting activity of QNP over Qu suggests that QNP may possess greater antidepressant potential.

In vivo Antidepressant Effect

Currently, multiple depression models are available for evaluating the in vivo antidepressant effects of drugs. One well-recognized classic model among these is the one established via CUMS. This model aligns with the pathogenesis and progression of human depression. Mice with successful CUMS modeling exhibit depressive-like symptoms. These symptoms include reduced interest in their surroundings, decreased activity levels, and anhedonia.[56,57] Therefore, after evaluating QNP's effects using multiple in vitro cellular depression models, we further assessed the in vivo antidepressant activity of QNP via the CUMS depression model. We used three behavioral tests to evaluate improvements in depressive symptoms in mice treated with QNP or Flu. These tests were the open field test, forced swim test, and sucrose preference test. As shown in Figure 8A, results from the open field test demonstrated that mice in the CUMS group exhibited a significant reduction in activity compared with those in the blank control group ($P < 0.0001$). This reduction was attributed to reduced interest in their surroundings (1871.29 ± 283.61 cm for blank control vs 908.84 ± 283.35 cm for CUMS, $P < 0.01$). After intervention with Flu or QNP, the activity of mice increased significantly. Moreover, low-dose QNP (10 mg/kg) induced a recovery in activity that was comparable to that of Flu (1523.99 ± 247.33 cm for QNP 10 mg/kg vs 1682.96 ± 237.49 cm for Flu, $P > 0.05$). As the QNP dose increased, mice in the 50 mg/kg QNP group showed a further increase in activity (1753.38 ± 291.27 cm). The forced swimming test assesses the will to survive in mice under extreme conditions. MDD mice remain immobile without struggling for extended periods during this test. This behavior is similar to the suicidal tendencies seen in patients with depression. As shown in Figure 8B, the immobility time of mice in the model group increased significantly after entering the water (81.33 ± 26.61s for the blank control group vs 209.15 ± 35.99s for the CUMS model group, $P < 0.05$). Each treatment group showed varying degrees of improvement, with significantly enhanced motivation to struggle. Among these groups, the immobility time of mice in the positive drug (Flu) group was close to that in the low-dose QNP group. The high-dose QNP group exhibited the strongest motivation to struggle, and the immobility time of these mice was improved more significantly ($P < 0.001$). This improvement was even close to that observed in the blank control group (106.80 ± 35.78s for the high-dose QNP group vs 81.33 ± 26.61s for the Flu group, $P > 0.05$). Additionally, the sucrose preference test is another tool used to evaluate depression in mice. Under normal feeding conditions, mice exhibit a preference for sugar water in this test. In contrast, depressive mice show no preference between sugar water and regular drinking water. This lack of preference is attributed to anhedonia and anorexia. As shown in Figure 8C, mice treated with QNP displayed a dose-dependent increase in sucrose preference. Specifically, the sucrose preference of the high-dose QNP group reached 71.81 ± 6.95%. Based on comprehensive behavioral tests and dynamic observations of mice, QNP exhibits antidepressant effects comparable to or even superior to those of Flu, which is a clinical first-line antidepressant.

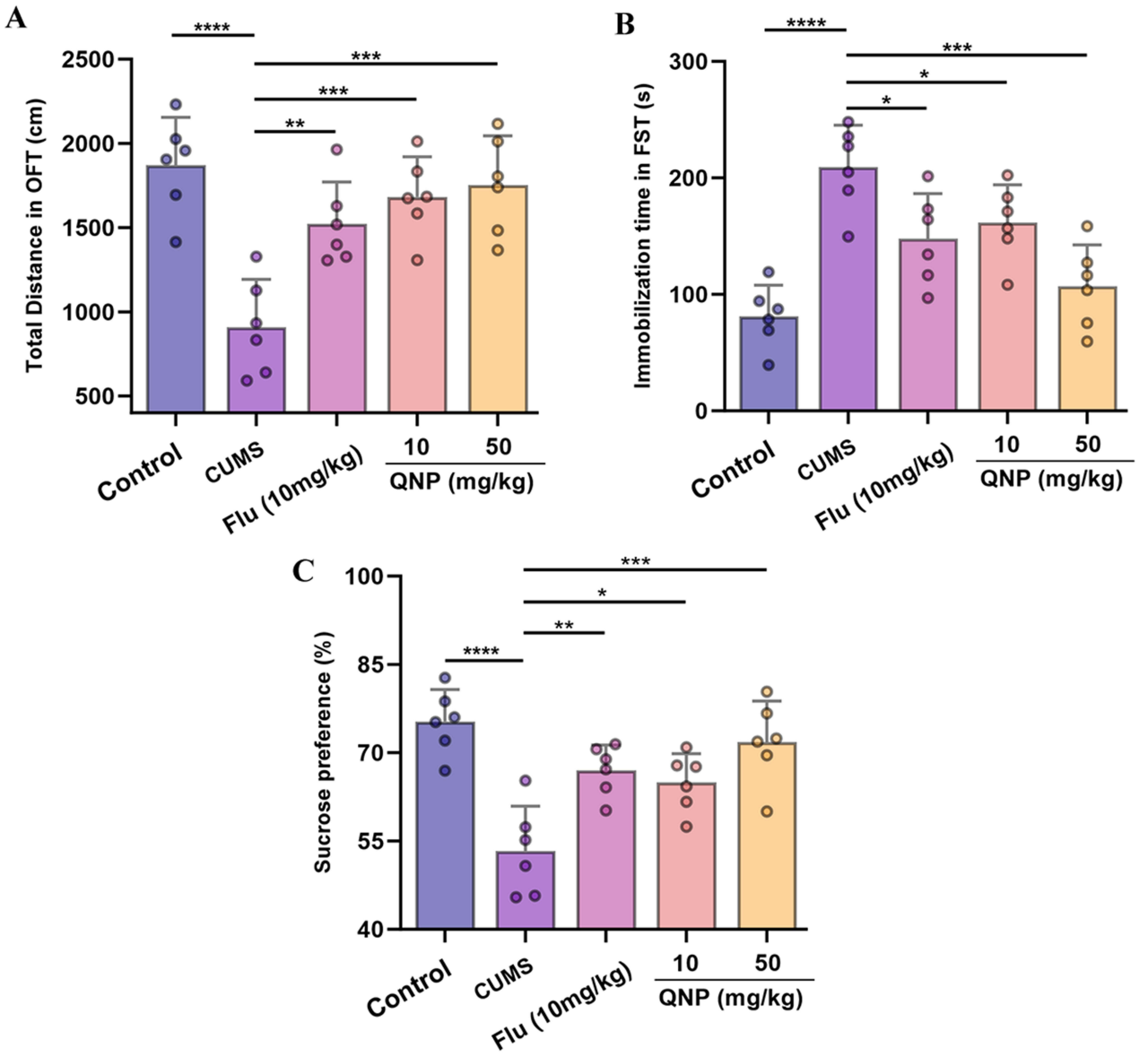

Figure 8 QNP exhibit a favorable therapeutic effect on ameliorating depressive-like behaviors in mice subjected to the CUMS depression model. (**A**) In the open field test (OFT), mice in the QNP-treated group exhibited a significant increase in total distance traveled. (**B**) In the forced swimming test (FST), mice in the QNP-treated group exhibited a significant decrease in immobility time. (**C**) In the sucrose preference test (SPT), mice in the QNP-treated group exhibited a significant increase in sucrose preference index. *$P < 0.05$, **$P < 0.01$, ***$P < 0.001$, ****$P < 0.0001$. * indicates the significance between the drug group or control group and the CUMS group at a specific concentration. ($\bar{x} \pm s$, n = 6).

Limitations

Although this study initially confirmed that QNP exerts enhanced antidepressant efficacy, it has certain limitations that require further refinement in future research. First, the focus of this study is to address the pharmaceutical challenges of quercetin, and the specific mechanism underlying QNP's antidepressant effect demands additional investigation. Second, regarding the cellular uptake pathway of QNP, while this study demonstrated that BV2 cells exhibit efficient uptake of QNP, the specific uptake mechanism remains to be further validated. Finally, this study confirmed QNP's potent antidepressant activity using the in vivo CUMS depression model, but the in vivo absorption and metabolic profiles of QNP will be a key focus of our subsequent research. For future practical applications, the potential long-term accumulation of nanoparticles in organs including the brain and liver must be considered, necessitating additional safety validation. Meanwhile, efforts are needed to address issues related to industrialization and clinical adaptability. We will

optimize the large-scale preparation process, resolve challenges in uniformity and stability control during QNP mass production, explore the clinical dosage range and administration frequency, and define the safe therapeutic window by integrating in vivo toxicity data.

Conclusions

Herein, a liposomal nano-delivery system QNP with enhanced brain delivery capability was designed and fabricated, which encapsulates the natural antidepressant active molecule Qu via Bor modification. Following confirmation of successful QNP preparation through structural characterizations (eg, particle size, PDI, Zeta potential, and TEM), QNP was found to not only possess sustained drug release capability but also exhibit enhanced cellular uptake efficiency. Preliminary findings from hemolysis and CCK-8 assays demonstrated favorable biocompatibility of QNP. Evaluations using CORT- and H_2O_2-induced cell injury models revealed that QNP exhibits greater antidepressant potential compared to free Qu. Moreover, following LPS-induced inflammatory responses in BV2 cells, QNP treatment significantly suppressed NO release, reduced ROS levels, and exerted more potent biological effects relative to Qu. In conclusion, this study developed QNP liposomal nanoparticles by integrating nanotechnology with active components from traditional Chinese medicine. This delivery system offers a promising strategy with favorable safety and targeting capability to enhance antidepressant efficacy, which is critical for advancing Qu from a dietary supplement to a precision antidepressant medication.

Abbreviations

BBB, Blood-brain barrier; BDNF, Brain-derived neurotrophic factor; Bor, Borneol; CNS, Central nervous system; CORT, Corticosterone; CUMS, Chronic unpredictable mild stress; Cy5.5, Cyanine5.5; DSPE-mPEG2000, 1,2-dis-tearoyl-sn-glycero-3-phosphoethanolamine-N-[methoxy (poly-ethylene glycol)-2000]; EE, Encapsulation efficiency; Flu, Fluoxetine; HE, Hematoxylin and eosin; HPA, Hypothalamic-pituitary-adrenal; HSPC, Hydrogenated soybean phospholipids; H_2O_2, Hydrogen peroxide; IL-1β, Interleukin-1β; LE, Loading efficiency; LPS, Lipopolysaccharide; MDD, Major depressive disorder; OD, Optical density; PBS, Phosphate buffered saline; PDI, polydispersity index; QNP, Quercetin-loaded nanoliposomes; Qu, Quercetin; ROS, Reactive oxygen species; TEM, Transmission electron microscopy.

Data Sharing Statement

Data and materials will be provided upon request and are available from the corresponding author.

Ethics Approval and Consent to Participate

The animal studies were done in compliance with the regulations and guidelines of laboratory animal welfare and ethics committee of Chongqing University Central Hospital and adhered to the ARRIVE guidelines. All animal experiments were approved (NO.2502002) by the Ethics Committee of Chongqing University Central Hospital.

Author Contributions

All authors made a significant contribution to the work reported, whether that is in the conception, study design, execution, acquisition of data, analysis and interpretation, or in all these areas; took part in drafting, revising or critically reviewing the article; gave final approval of the version to be published; have agreed on the journal to which the article has been submitted; and agree to be accountable for all aspects of the work.

Funding

This study was supported by the Yibin Science and Technology Plan Project (No.2025MZ008) and the Chongqing medical scientific research project (Joint project of Chongqing Health Commission and Science and Technology Bureau, No.2025QNXM019).

Disclosure

The authors declare no conflict of interest.

References

1. Diseases GBD, Injuries C. Global incidence, prevalence, years lived with disability (YLDs), disa bility-adjusted life-years (DALYs), and healthy life expectancy (HALE) for 371 diseases and injuries in 204 countries and territories and 81 1 subnational locations, 1990-2021: a systematic analysis for the global burden of disease study 2021. *Lancet*. 2024;403(10440):2133–2161. doi:10.1016/S0140-6736(24)00757-8
2. Lagerberg T, Matthews AA, Zhu N, Fazel S, Carrero -J-J, Chang Z. Effect of selective serotonin reuptake inhibitor treatment following diagnosis of depression on suicidal behaviour risk: a target trial emulation. *Neuropsychopharmacology*. 2023;48(12):1760–1768. doi:10.1038/s41386-023-01676-3
3. Protti M, Mandrioli R, Marasca C, Cavalli A, Serretti A, Mercolini L. New-generation, non-SSRI antidepressants: drug-drug interactions and therapeutic drug monitoring. Part 2: naSSAs, NRIs, SNDRIs, MASSAs, NDRIs, and others. *Med Res Rev*. 2020;40(5):1794–1832. doi:10.1002/med.21671
4. Abram SV, Roach BJ, Fryer SL, et al. Validation of ketamine as a pharmacological model of thalamic dysconnectivity across the illness course of schizophrenia. *Mol Psychiatry*. 2022;27(5):2448–2456. doi:10.1038/s41380-022-01502-0
5. Paolicelli RC, Sierra A, Stevens B, et al. Microglia states and nomenclature: a field at its crossroads. *Neuron*. 2022;110(21):3458–3483. doi:10.1016/j.neuron.2022.10.020
6. Augusto-Oliveira M, Arrifano G, Leal-Nazaré CG, et al. Morphological diversity of microglia: implications for learning, environmental adaptation, ageing, sex differences and neuropathology. *Neurosci Biobehav Rev*. 2025;172:106091. doi:10.1016/j.neubiorev.2025.106091
7. Zeng Y, Chourpiliadis C, Hammar N, et al. Inflammatory biomarkers and risk of psychiatric disorders. *JAMA Psychiatry*. 2024;81(11):1118–1129. doi:10.1001/jamapsychiatry.2024.2185
8. Liu Y, Zhang B, Zhou Y, et al. Plasma oxidative stress marker levels related to functional brain abnormalities in first-episode drug-naive major depressive disorder. *Psychiatry Res*. 2024;333:115742. doi:10.1016/j.psychres.2024.115742
9. Bhatt S, Nagappa AN, Patil CR. Role of oxidative stress in depression. *Drug Discov Today*. 2020;25(7):1270–1276. doi:10.1016/j.drudis.2020.05.001
10. Guan T, Cao C, Hou Y, et al. Effects of quercetin on the alterations of serum elements in chronic unpredictable mild stress-induced depressed rats. *Biometals*. 2021;34(3):589–602. doi:10.1007/s10534-021-00298-w
11. Li Y, Yao J, Han C, et al. Inflammation and Immunity. *Nutrients*. 2016;8(3):167. doi:10.3390/nu8030167
12. Abdulla Kadhim R, Ahmed Rahmah A-R, Alaa Hamza A, Hayder R-S, Enass Najem OJ. Quercetin mitigates sepsis-induced renal injury via inhibiting inflammatory and oxidative pathways in mice. *J Mol Histol*. 2025;56(3):184. doi:10.1007/s10735-025-10442-2
13. Frenț O-D, Stefan L, Morgovan CM, et al. A systematic review: quercetin-secondary metabolite of the flavonol class, with multiple health benefits and low bioavailability. *Int J Mol Sci*. 2024;25(22):12091. doi:10.3390/ijms252212091
14. Han X, Xu T, Fang Q, et al. Quercetin hinders microglial activation to alleviate neurotoxicity via the interplay between NLRP3 inflammasome and mitophagy. *Redox Biol*. 2021;44:102010. doi:10.1016/j.redox.2021.102010
15. Agrawal K, Chakraborty P, Dewanjee S, et al. Neuropharmacological interventions of quercetin and its derivatives in neurological and psychological disorders. *Neurosci Biobehav Rev*. 2023;144:104955. doi:10.1016/j.neubiorev.2022.104955
16. Naeem A, Ming Y, Pengyi H, et al. The fate of flavonoids after oral administration: a comprehensive overview of its bioavailability. *Crit Rev Food Sci Nutr*. 2022;62(22):6169–6186. doi:10.1080/10408398.2021.1898333
17. Li H, Li M, Fu J, Ao H, Wang W, Wang X. Enhancement of oral bioavailability of quercetin by metabolic inhibitory nanosuspensions compared to conventional nanosuspensions. *Drug Deliv*. 2021;28(1):1226–1236. doi:10.1080/10717544.2021.1927244
18. Pinheiro RGR, Pinheiro M, Neves AR. Nanotechnology innovations to enhance the therapeutic efficacy of quercetin. *Nanomaterials*. 2021;11(10):2658. doi:10.3390/nano11102658
19. Vengadesan D, Arumugam N, Manikandan E, Mandal A. Evaluation of nanomaterials as effective carriers targeted to traverse blood–brain barrier for theragnostics of neurodegenerative diseases: an overview. *BioNanoScience*. 2025;15(1):143. doi:10.1007/s12668-024-01773-7
20. O'Brien Laramy M, Foley DA, Pak RH, et al. Chemistry, manufacturing and controls strategies for using novel excipients in lipid nanoparticles. *Nat Nanotechnol*. 2025;20(3):331–344. doi:10.1038/s41565-024-01833-9
21. Seyyedi-Mansour S, Carpena M, Barciela P, et al. Lipid-based nanocarriers loaded with bioactive compounds in active food packaging: fabrication, characterization, and applications. *Adv Colloid Interface Sci*. 2025;340:103457. doi:10.1016/j.cis.2025.103457
22. Pei J, Kumarasamy RV, Jayaraman S, Kanniappan GV, Long Q, Palanisamy CP. Quercetin-functionalized nanomaterials: innovative therapeutic avenues for Alzheimer's disease management. *Ageing Res Rev*. 2025;104:102665. doi:10.1016/j.arr.2025.102665
23. Lüdtke FL, Silva TJ, da Silva MG, Hashimoto JC, Ribeiro APB. Lipid nanoparticles: formulation, production methods and characterization protocols. *Foods*. 2025;14(6):973. doi:10.3390/foods14060973
24. Shah RM, Jadhav SR, Bryant G, Kaur IP, Harding IH. On the formation and stability mechanisms of diverse lipid-based nanostructures for drug delivery. *Adv Colloid Interface Sci*. 2025;338:103402. doi:10.1016/j.cis.2025.103402
25. Hu X, Yan Y, Liu W, et al. Advances and perspectives on pharmacological activities and mechanisms of the monoterpene borneol. *Phytomedicine*. 2024;132:155848. doi:10.1016/j.phymed.2024.155848
26. Liu S, Long Y, Yu S, et al. Borneol in cardio-cerebrovascular diseases: pharmacological actions, mechanisms, and therapeutics. *Pharmacol Res*. 2021;169:105627. doi:10.1016/j.phrs.2021.105627
27. Wang Y, Ma X, Wang X, et al. Traditional Chinese medicine borneol-based polymeric micelles intracer ebral drug delivery system for precisely pathogenesis-adaptive treatment of ischemic stroke. *Adv Sci*. 2025;12(9):e2410889. doi:10.1002/advs.202410889
28. Long Y, Liu S, Wan J, et al. Brain targeted borneol-baicalin liposome improves blood-brain barrier integrity after cerebral ischemia-reperfusion injury via inhibiting HIF-1α/VEGF/eNOS/NO signal pathway. *Biomed Pharmacother*. 2023;160:114240. doi:10.1016/j.biopha.2023.114240
29. Amidon GE, Higuchi WI, Ho NF. Theoretical and experimental studies of transport of micelle-solubilized solutes. *J Pharm Sci*. 1982;71(1):77–84. doi:10.1002/jps.2600710120
30. Smith OEP, Waters LJ, Small W, Mellor S. CMC determination using isothermal titration calorimetry for five industrially significant non-ionic surfactants. *Colloids Surf B Biointerfaces*. 2022;211:112320. doi:10.1016/j.colsurfb.2022.112320
31. Abbot V, Sharma P. Investigation of interactions between quercetin and Tween 80 through electrolyte induced thermodynamic approach. *Mater Today Proc*. 2020; 28:61–64.
32. Vigneshwari R, Dash S. Comparative interaction of flavonoid quercetin with different tween surfactants. *ACS Food Sci Tech*. 2023;3(5):969–980. doi:10.1021/acsfoodscitech.3c00105

33. Wang D, Yu Z, Yao R, et al. Quercetin alleviates depressive-like behavior by modulating acetyl-H3K9 mediated ferroptosis pathway in hypothalamus of perimenopausal depression rat model. *Biomed Pharmacother*. 2024;179:117369. doi:10.1016/j.biopha.2024.117369
34. Zhang Y, Wang B, Liu L, et al. The mechanistic study of quercetin in the treatment of alcoholic brain injury via the JNK/P38 MAPK signaling pathway. *Apoptosis*. 2025;30(7–8):1875–1892. doi:10.1007/s10495-025-02125-w
35. Fan Y, Marioli M, Zhang K. Analytical characterization of liposomes and other lipid nanoparticles for drug delivery. *J Pharm Biomed Anal*. 2021;192:113642. doi:10.1016/j.jpba.2020.113642
36. Le K, Song Z, Deng J, et al. Quercetin alleviates neonatal hypoxic-ischemic brain injury by inhibiting microglia-derived oxidative stress and TLR4-mediated inflammation. *Inflamm Res*. 2020;69(12):1201–1213. doi:10.1007/s00011-020-01402-5
37. Zhao X, Ni S, Song Y, Hu K. Intranasal delivery of Borneol/R8dGR peptide modified PLGA nanoparticles co-loaded with curcumin and cisplatin alleviate hypoxia in pediatric brainstem glioma which improves the synergistic therapy. *J Control Release*. 2023;362:121–137. doi:10.1016/j.jconrel.2023.08.048
38. Wang G, Cao L, Li S, et al. Corticosterone impairs hippocampal neurogenesis and behaviors through p21-mediated ROS accumulation. *Biomolecules*. 2024;14(3):268. doi:10.3390/biom14030268
39. Zhang K, Wang F, Zhai M, et al. Hyperactive neuronal autophagy depletes BDNF and impairs adult hippocampal neurogenesis in a corticosterone-induced mouse model of depression. *Theranostics*. 2023;13(3):1059–1075. doi:10.7150/thno.81067
40. Murray F, Smith DW, Hutson PH. Chronic low dose corticosterone exposure decreased hippocampal cell proliferation, volume and induced anxiety and depression like behaviours in mice. *Eur J Pharmacol*. 2008;583(1):115–127. doi:10.1016/j.ejphar.2008.01.014
41. Zhao J, Gao X, Wang A, et al. Depression comorbid with hyperalgesia: different roles of neuroinflammation induced by chronic stress and hypercortisolism. *J Affect Disord*. 2019;256:117–124. doi:10.1016/j.jad.2019.05.065
42. Salim S. Oxidative stress and psychological disorders. *Curr Neuropharmacol*. 2014;12(2):140–147. doi:10.2174/1570159X11666131120230309
43. Winczewska Z, Mechlińska A, Radziwiłłowicz P, et al. Estrogen metabolites and hydrogen peroxide - Missing elements in the pathophysiology and possible treatment of treatment-resistant depression? *Redox Biol*. 2025;81:103547. doi:10.1016/j.redox.2025.103547
44. Rybka J, Kędziora-Kornatowska K, Banaś-Leżańska P, et al. Interplay between the pro-oxidant and antioxidant systems and proinflammatory cytokine levels, in relation to iron metabolism and the erythron in depression. *Free Radic Biol Med*. 2013;63:187–194. doi:10.1016/j.freeradbiomed.2013.05.019
45. Jomova K, Raptova R, Alomar SY, et al. Reactive oxygen species, toxicity, oxidative stress, and antioxidants: chronic diseases and aging. *Arch Toxicol*. 2023;97(10):2499–2574. doi:10.1007/s00204-023-03562-9
46. Ding Q, Li D, Zhang X, et al. Restoring the redox and norepinephrine homeostasis in mouse brains promotes an antidepressant response. *J Am Chem Soc*. 2025;147(13):11239–11249. doi:10.1021/jacs.4c18046
47. Nisticò R, Piccirilli S, Cucchiaroni ML, et al. Neuroprotective effect of hydrogen peroxide on an in vitro model of brain ischaemia. *Br J Pharmacol*. 2008;153(5):1022–1029. doi:10.1038/sj.bjp.0707587
48. Ogura Y, Sato K, Kawashima K-I, et al. Subtoxic levels of hydrogen peroxide induce brain-derived neurotrophic factor expression to protect PC12 cells. *BMC Res Notes*. 2014;7(1):840. doi:10.1186/1756-0500-7-840
49. Liu D, Wang Z, Liu S, Wang F, Zhao S, Hao A. Anti-inflammatory effects of fluoxetine in lipopolysaccharide(LPS)-stimulated microglial cells. *Neuropharmacology*. 2011;61(4):592–599. doi:10.1016/j.neuropharm.2011.04.033
50. Yoshioka Y, Takeda N, Yamamuro A, Kasai A, Maeda S. Nitric oxide inhibits lipopolysaccharide-induced inducible nitric oxide synthase expression and its own production through the cGMP signaling pathway in murine microglia BV-2 cells. *J Pharmacol Sci*. 2010;113(2):153–160. doi:10.1254/jphs.10060FP
51. Tavakol F, Amini-Khoei H, Sureda A, Zarean E, Lorigooini Z. Exploring the anti-depressant effects and nitric oxide modulation of quercetin: a preclinical study in socially isolated mice. *World J Biol Psychiatry*. 2024;25(10):592–603. doi:10.1080/15622975.2024.2424162
52. Mandal A, Krishnan RSG, Thennarasu S, Panigrahi S, Mandal AB. Two-dimensional surface properties of an antimicrobial hydantoin at the air–water interface: an experimental and theoretical study. *Colloids Surf B*. 2010;79(1):136–141. doi:10.1016/j.colsurfb.2010.03.042
53. Jankovic T, Bogicevic M, Knezevic NN. The role of nitric oxide and hormone signaling in chronic stress, anxiety, depression and post-traumatic stress disorder. *Mol Cell Endocrinol*. 2024;590:112266. doi:10.1016/j.mce.2024.112266
54. Sun Y, Zhang H, Wu Z, et al. Quercitrin rapidly alleviated depression-like behaviors in lipopolysac charide-treated mice: the involvement of PI3K/AKT/NF-κB signaling suppression and CREB/BDNF signaling restoration in the hippocampus. *ACS Chem Neurosci*. 2021;12(18):3387–3396. doi:10.1021/acschemneuro.1c00371
55. Tang J, Diao P, Shu X, Li L, Xiong L. Quercetin and quercitrin attenuates the inflammatory response and oxidative stress in LPS-induced RAW264.7 cells: in vitro assessment and a theoretical model. *Biomed Res Int*. 2019;2019:7039802. doi:10.1155/2019/7039802
56. Antoniuk S, Bijata M, Ponimaskin E, Wlodarczyk J. Chronic unpredictable mild stress for modeling depression in rodents: meta-analysis of model reliability. *Neurosci Biobehav Rev*. 2019;99:101–116. doi:10.1016/j.neubiorev.2018.12.002
57. Ratajczak P, Martyński J, Zięba JK, et al. Comparative efficacy of animal depression models and antidepressant treatment: a systematic review and meta-analysis. *Pharmaceutics*. 2024;16(9):1144. doi:10.3390/pharmaceutics16091144